JOURNAL OF COMPUTATIONAL PHYSICS 117, 183–193 (1995)

Space-Time Integrated Least-Squares: Solving a Pure Advection Equation with a Pure Diffusion Operator

PIERRE PERROCHET AND PASCAL AZÉRAD

Université de Neuchâtel, CH-2007 Neuchâtel, Switzerland

Received February 15, 1994

An alternative formulation for multidimensional scalar advection is derived following both a conservative and a variational approach, by applying the least-squares method simply generalized to the space-time domain. In the space-time framework pure advection is regarded as a process involving only anisotropic diffusion along space-time characteristics. The resulting parabolic-type equation lends itself to a straightforward Galerkin integration that yields a symmetric, diagonally dominant, positive, and unconditionally stable operator. The conditions of equivalence between the advective problem and its parabolized counterpart are established by using standard variational theory in anisotropic Sobolev spaces specially designed for advection equations. To demonstrate the general applicability of the method, "parabolized advection" is simulated in 2D manifolds embedded in 3D and 4D space-time domains.

1. INTRODUCTION

Numerous attempts have been made during the past two decades to improve the numerical solution of the deemed complex advection equation. Among various successful techniques, and unlike a few promising least-squares finite element schemes [1–2], the early Petrov- and Taylor-Galerkin schemes have now become sophisticated enough to provide analysts with very accurate solvers for first order hyperbolic test problems [3, 4, 7–10].

However, when applied to transient problems involving nonhomogeneous flow fields, sharp fronts, irregular meshes, and/or relatively coarse time discretization, these methods may lose some of their good performances (i.e., stability, accuracy, and robustness). One major source of problems being the different discretization of space and time, which prevents the information from following the characteristics properly, as discussed in [8, 14].

In this work we develop and analyze the space-time integrated least-squares (STILS) approach. In doing so we replace the advective operator by a diffusive equivalent and adopt a time-augmented Galerkin framework in order to achieve proper implementation of the resulting space-time tensor functions. Apart from simply allowing use of computationally safe, steady-state elliptic Galerkin algorithms to solve advective problems, the present work addresses also a single concept that may be relevant to both numerical analysis and physics. As will be shown further on, a streamline diffusion process along the space-time characteristics arises here naturally from a physical conservation law and a variational principle, and not from the specific structure of an integration method of Petrov–Galerkin type. Moreover, the space-time setting allows us to take full advantage of the stabilizing properties of the least-squares method (see [17]), which makes it possible to convert the hyperbolic advection equation into its parabolic diffusion counterpart.

In a way, our method can be seen as a variant of the recent characteristic streamline diffusion (CSD) [11, 12], Galerkin least squares (GLS) [5] or of the streamline upwind full galerkin (SUFG) [14] methods, but of an easier implementation, because we neither introduce any extra parameter to be carefully selected, nor use discontinuous in time elements. It is also conceptually simpler, because we take full advantage of the space time framework. However, STILS only works for pure advection equations, whereas SUFG can also tackle advection-diffusion ones, and GLS or CSD general symmetric advective-diffusive systems such as, e.g, Navier–Stokes equations (see [6, 13]).

2. ALTERNATIVE FORMULATION OF ADVECTION

For simplicity, but without loss of generality, we consider below the source free, scalar advection equation commonly expressed as

$$\frac{\partial u}{\partial t} = -\mathbf{v} \cdot \nabla u \tag{1}$$

with advective velocity field $\mathbf{v} = (v_x, v_y, v_z)$ function of space and time coordinates and subject to upstream Dirichlet boundary conditions. Equation (1)—which obviously considers space and time as two distinct domains—implies that time variations of the unknown concentration function u are zero when $\mathbf{v}$ is perpendicular to ∇u (steady-state regime) and are maximum when these two vectors are parallel.

The underlying trivial condition governing space-time advection may, however, be better expressed when considering the 4D continuum. In effect, upon defining

0021-9991/95 $6.00

$$\tilde{\nabla} = (\nabla, \partial_t), \quad \tilde{\mathbf{v}} = (\mathbf{v}, v_t = 1), \tag{2}$$

Eq. (1) takes the form

$$\tilde{\mathbf{v}} \cdot \tilde{\nabla} u = 0 \tag{3}$$

which clearly expresses the orthogonality of space-time gradients and characteristics throughout the space-time domain. Equation (3) may then be solved using appropriate steady-state algorithms designed to cure the oscillating behavior of numerical solutions to hyperbolic problems. As an alternative to this, a parabolic streamline diffusion equation is developed below following two distinct lines of reasoning.

Conservative Approach

A possibility to transform the problem in Eq. (3) is to define the quantity

$$\tilde{\mathbf{q}} = (\tilde{\mathbf{v}} \cdot \tilde{\nabla} u)\tilde{\mathbf{v}} = [\tilde{\mathbf{v}} \otimes \tilde{\mathbf{v}}]\, \tilde{\nabla} u \tag{4}$$

which represents a space-time streamline diffusive flux (in the above equation the sign $\otimes$ denotes a tensor product thus making $[\tilde{\mathbf{v}} \otimes \tilde{\mathbf{v}}]$ a 4×4-matrix). Specifying then "steady-state" zero divergence for the above equation yields the conservative statement

$$\tilde{\nabla} \cdot ([\tilde{\mathbf{v}} \otimes \tilde{\mathbf{v}}]\, \tilde{\nabla} u) = 0. \tag{5}$$

According to Eq. (5)—where $\tilde{\mathbf{v}} \otimes \tilde{\mathbf{v}}$ is seen as an anisotropic "diffusion" tensor—the basic advective process may now be regulated by a diffusive-type equation with diffusion acting only in the direction of $\tilde{\mathbf{v}}$. In order to reproduce the advective effects and the related full penetration of the upstream Dirichlet "hard" boundary conditions (on space-time inflow boundaries Γ_1) into the flow domain, zero Neumann "soft" conditions have to be enforced on downstream boundaries (on space-time outflow boundaries Γ_2). We define precisely these boundaries below. Hence, and as illustrated in Fig. 1, the solution of Eq. (5) will consist of constant concentration along space-time characteristics and Eq. (3) will be implicitly satisfied.

Variational Approach

Another and perhaps more rigorous way to derive Eq. (5) with the associated boundary conditions is to perform an integral variational analysis. Instead of focusing on Eq. (3) we might as well consider the least-squares function

$$\pi = \frac{1}{2}\int_\Omega (\tilde{\mathbf{v}} \cdot \tilde{\nabla} u)^2, \tag{6}$$

where Ω is the space-time domain and for which Eq. (3) obviously yields the absolute minimum $\pi = 0$.

The minimization of a generalized least-squares statement

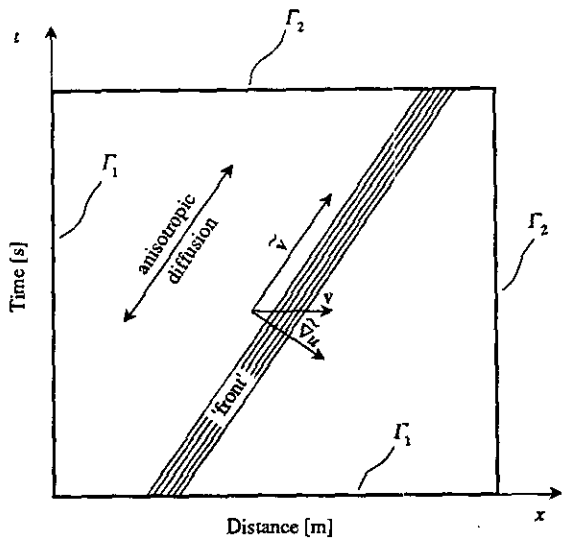

FIG. 1. Representation of advection with up and down-stream boundaries Γ_1 and Γ_2 in space-time.

for an advection-diffusion equation has already been reported in [1]. However, due to the presence of diffusion and to unusual space-time approximations, the developments performed in this early work are different and somewhat less straightforward.

In effect, minimizing the above functional gives

$$\delta\pi = \int_\Omega (\tilde{\mathbf{v}} \cdot \tilde{\nabla} u)\, \delta(\tilde{\mathbf{v}} \cdot \tilde{\nabla} u) = \int_\Omega (\tilde{\mathbf{v}} \cdot \tilde{\nabla} u)(\tilde{\mathbf{v}} \cdot \tilde{\nabla}\, \delta u) \tag{7}$$
$$= \int_\Omega \tilde{\nabla}\, \delta u \cdot [\tilde{\mathbf{v}} \otimes \tilde{\mathbf{v}}]\, \tilde{\nabla} u = 0$$

an integration by parts results in

$$\delta\pi = \int_\Gamma \delta u([\tilde{\mathbf{v}} \otimes \tilde{\mathbf{v}}]\, \nabla u) \cdot \tilde{\mathbf{n}} - \int_\Omega \delta u\, \tilde{\nabla} \cdot ([\tilde{\mathbf{v}} \otimes \mathbf{v}]\, \tilde{\nabla} u) = 0, \tag{8}$$

where $\tilde{\mathbf{n}}$ is the outer normal unit vector to the space-time boundary Γ. Defining now the space-time in- and out-flow boundaries, $\Gamma_1 = \{(x, t) \in \Gamma | \tilde{\mathbf{v}} \cdot \tilde{\mathbf{n}} < 0\}$, $\Gamma_2 = \{(x, t) \in \Gamma | \tilde{\mathbf{v}} \cdot \tilde{\mathbf{n}} > 0\}$, we get that a minimum of (6) is obtained when

$$\tilde{\nabla} \cdot ([\tilde{\mathbf{v}} \otimes \tilde{\mathbf{v}}]\, \tilde{\nabla} u) = 0, \quad \text{in } \Omega$$

with

$$\begin{aligned} u &= u_0 \quad (\text{i.e., } \delta u = 0), \quad \text{on } \Gamma_1 \\ [\tilde{\mathbf{v}} \otimes \tilde{\mathbf{v}}]\, \tilde{\nabla} u \cdot \tilde{\mathbf{n}} &= 0, \quad \text{on } \Gamma_2 \end{aligned} \tag{9}$$

We note here that the Neumann-type condition on Γ_2 may also be expressed by

$$\tilde{\mathbf{v}} \otimes \tilde{\mathbf{v}}\, \tilde{\nabla} u \cdot \tilde{\mathbf{n}} = \tilde{\mathbf{v}} \otimes \tilde{\mathbf{v}} \tilde{\mathbf{n}} \cdot \tilde{\nabla} u = (\tilde{\mathbf{v}} \cdot \tilde{\mathbf{n}}) \tilde{\mathbf{v}} \cdot \tilde{\nabla} u = 0$$

and, since $(\tilde{\mathbf{v}} \cdot \tilde{\mathbf{n}})\tilde{\mathbf{v}} // \tilde{\mathbf{v}}$, this condition means that $\tilde{\mathbf{v}} \cdot \tilde{\nabla} u = 0$ on Γ_2 and also on Γ_1 (where $\tilde{\mathbf{v}} \cdot \tilde{\mathbf{n}} \neq 0$) which only reflects mass conservation. Moreover, it is evident that the above Neumann-type condition also applies to the other domain no-flow boundaries ($\Gamma - \Gamma_1 - \Gamma_2$), where $\tilde{\mathbf{v}} \cdot \tilde{\mathbf{n}} = 0$.

The equivalence of the classical advection problem with the STILS-based formulation given in (9) is demonstrated below.

3. EQUIVALENCE OF ADVECTIVE AND DIFFUSIVE FORMULATIONS

In this section we consider Ω as a n-dimensional domain ($n = 4$ for space-time) and we omit tildes on space-time vectors. Moreover, without restricting the generality of the demonstration, we may take an homogeneous Dirichlet boundary condition by introducing a source term that we denote by f. We shall then study the equivalence between the following two formulations, namely the advective one,

$$\begin{aligned} \mathbf{v} \cdot \nabla u &= f, \quad \text{in } \Omega \\ u &= 0, \quad \text{on } \Gamma_1 \end{aligned} \tag{10}$$

and the diffusive one

$$\begin{aligned} \nabla \cdot ([\mathbf{v} \otimes \mathbf{v}]\, \nabla u) &= \nabla \cdot (f\mathbf{v}), \quad \text{in } \Omega \\ u &= 0, \quad \text{on } \Gamma_1 \\ [\mathbf{v} \otimes \mathbf{v}]\mathbf{n} \cdot \nabla u &= f\mathbf{v} \cdot \mathbf{n}, \quad \text{on } \Gamma - \Gamma_1. \end{aligned} \tag{11}$$

Let us note that the downstream boundary condition arises *naturally* from the variational formulation. As for the upstream Dirichlet boundary condition, let us point out that in the space-time context it covers both the initial condition and the classical spatial Dirichlet condition. We need some unusual function spaces especially tailored for the problem. To this end we define

$$H(\mathbf{v}, \Omega) = \{u \in L^2(\Omega): \mathbf{v} \cdot \nabla u \in L^2(\Omega)\}$$

equipped with the norm

$$|||u|||^2 = \|u\|^2 + \|\mathbf{v} \cdot \nabla u\|^2,$$

where $\|\cdot\|$ designates the usual L^2 norm and $\mathbf{v} \cdot \nabla u$ is to be interpreted in the generalized sense as a distribution.

Like for standard Sobolev spaces, one easily shows that $H(\mathbf{v}, \Omega)$ is a Hilbert space. To take into account the homogeneous Dirichlet boundary condition, we define

$$H_0(\mathbf{v}, \Omega, \Gamma_1) = \{u \in H(\mathbf{v}, \Omega): u = 0 \text{ on } \Gamma_1\}.$$

Remark 1. In order to make this definition perfectly valid we would need to give some sense to u on Γ_1. Indeed one can build a trace like operator $\theta: H(\mathbf{v}, \Omega) \to H^{-1/2}(\partial\Omega)$ such that $\theta(u) = u\ \mathbf{v} \cdot \mathbf{n}$ for smooth u. This has already been done in the case of constant $\mathbf{v}$ [16] and can be extended to cover the general case if Ω is regular enough.

The weak formulation of the diffusive problem (11) is:

Find $u \in H_0(\mathbf{v}, \Omega, \Gamma_1)$ such that for all $\phi \in H_0(\mathbf{v}, \Omega, \Gamma_1)$

$$\int_\Omega (\mathbf{v} \cdot \nabla u)(\mathbf{v} \cdot \nabla \phi) = \int_\Omega f(\mathbf{v} \cdot \nabla \phi). \tag{12}$$

First of all, it is obvious that if $u \in L^2(\Omega)$ is the solution of (10) then u satisfies (12). To see that, one performs the L^2 dot-product of (10) by $\mathbf{v} \cdot \nabla \phi$ for an arbitrary $\phi \in H_0(\mathbf{v}, \Omega, \Gamma_1)$. As an hypothesis we shall need the following "curved" Poincaré style inequality

$$\exists\, C \text{ such that } \forall u \in H_0(\mathbf{v}, \Omega, \Gamma_1), \quad \|u\| \leq C \|\mathbf{v} \cdot \nabla u\|. \tag{13}$$

Remark 2. This inequality is satisfied, for instance, when $\mathbf{v}$ is constant and when the characteristics starting from Γ_1 (for example, straight lines parallel to $\mathbf{v}$ as in Fig. 1) fill the whole domain Ω, which is only natural if the advection problem (10) is to be well posed. In fact, more generally if (10) is well posed we have the stability inequality

$$\|u\| \leq C \|f\|, \quad \text{i.e., } \|u\| \leq C \|\mathbf{v} \cdot \nabla u\|.$$

Sufficient and physically clear conditions for inequality (13) to be fulfilled are under investigation. The main theorem follows.

THEOREM. *If $f \in L^2(\Omega)$ and if the curved Poincaré inequality* (13) *is fulfilled, problem* (12) *is well posed.*

Proof. On $V = H_0(\mathbf{v}, \Omega, \Gamma_1)$, define the symmetric bilinear form a and the linear form l by

$$a(u, \phi) = \int_\Omega (\mathbf{v} \cdot \nabla u)(\mathbf{v} \cdot \nabla \phi), \quad l(\phi) = \int_\Omega f(\mathbf{v} \cdot \nabla \phi).$$

They are obviously continuous on V. Moreover, the bilinear form is coercive, thanks to inequality (13), namely

$$\begin{aligned} a(u, u) = \|\mathbf{v} \cdot \nabla u\|^2 &\geq \frac{1}{2} \left\| \mathbf{v} \cdot \nabla u \right\|^2 + \frac{C^2}{2} \|u\|^2 \\ &\geq \min\left(\frac{1}{2}, \frac{C^2}{2}\right) |||u|||^2. \end{aligned}$$

By the Lax–Milgram lemma, there is a unique solution to (12) and $|||u||| \leq C \|f\|$, with C a suitable constant. Q.E.D.

Applying this theorem to a finite element subspace V_h of $H_0(\mathbf{v}, \Omega, \Gamma_1)$, we obtain the well-posedness of the STILS method presented in this work.

Let us close this section with a principle *example* illustrating the applicability of the method. Consider the following classical formulation of the scalar transient advection problem with constant velocity v, namely,

$$\begin{aligned} vu_x + u_t &= f \qquad \text{on }]a, b[\times]0, T[\\ u(x, 0) &= g(x), \quad x \in]a, b[\\ u(a, t) &= h(t), \quad t \in]0, T[\end{aligned}$$

for which the diffusive formulation (11) is

$$\begin{aligned} v^2 u_{xx} + 2v u_{xt} + u_{tt} &= v f_x + f_t \quad \text{on }]a, b[\times]0, T[\\ u(x, 0) &= g(x), \quad x \in]a, b[\\ u(a, t) &= h(\mathrm{t}), \quad t \in]0, T[\\ vu_x + u_t &= f, \quad \text{at } t = T, x \in]a, b[; \\ & \quad x = b, t \in]0, T[\end{aligned}$$

In this case inequality (13) is satisfied (Remark 2), since characteristics starting from the inflow boundary Γ_1 fill the whole domain (as in Fig. 1), hence allowing proper use of the STILS method.

Conclusion. Under the assumption that the "curved" Poincaré inequality (13) is fulfilled, we solved the multidimensional linear, transient, or stationary scalar advection equation by replacing it by a diffusion one, the weak form of which is controlled by a coercive bilinear form in a suitable function space.

4. STANDARD GALERKIN INTEGRATION ANALYSIS

The problem expressed in (9) is now discretized using the Galerkin method. Time is represented by the Cartesian space variable ζ through the mapping

$$\zeta = \beta t, \tag{14}$$

where β is a conversion factor. With the change of variable (14) the terms in Eq. (9) are redefined as

$$\tilde{\nabla} = \left(\nabla, \partial_\zeta = \frac{1}{\beta}\partial_t\right), \quad \tilde{\mathbf{v}} = (\mathbf{v}, v_\zeta = \beta). \tag{15}$$

The introduction of the factor β in the system is important. When the space-time domain is subdivided in finite elements the size $\Delta\zeta$ given to the elements is generally fixed but can represent arbitrary time steps Δt. In order to preserve a consistent metric for the calculations of space-time gradients and trajectories it is therefore necessary to respect the transformation (14) and to calculate

$$\beta = \Delta\zeta/\Delta t \tag{16}$$

before assembling the Galerkin finite element equations (see also [14, 15]).

Matrix Equations

On each element defined by m nodes the unknown function u is approximated by

$$u = \sum_{n=1}^{m} \tilde{N}_n u_n = \tilde{\mathbf{N}}^{\mathrm{T}}\mathbf{u}, \quad \tilde{N}_n = \tilde{N}_n(x, y, z, \zeta) \tag{17}$$

and the classical weighted residual method applied to our problem yields the element divergence matrix

$$\tilde{A}^e_{ik} = \sum_i \left(\sum_j \int_{\Omega^e} \frac{\partial \tilde{N}_i}{\partial x^i} \tilde{v}^i \tilde{v}^j \frac{\partial \tilde{N}_k}{\partial x^j} d\Omega \right), \tag{18}$$

where superscripts i and j are relative to space-time Cartesian coordinates or, more synthetically,

$$\tilde{\mathbf{A}}^e = \{\tilde{\nabla}\tilde{\mathbf{N}}^T[\tilde{\mathbf{v}} \otimes \tilde{\mathbf{v}}]\,\tilde{\nabla}\tilde{\mathbf{N}}\}, \tag{19}$$

where the brackets { } summarize the operations of element integration.

One notes here that the structure of the term (19) could also be obtained with a Petrov–Galerkin type integration of an advective term, but in this case the weighting function would only consist of an asymmetric anisotropic perturbation $\tilde{\mathbf{v}} \cdot \tilde{\nabla}\tilde{\mathbf{N}}$. Hence the present formulation is similar to the space-time GLS method [5], the CSD method [11], or the SUFG method [14] in which the major term (i.e., the advection) would be suppressed!

The assembly of element matrix $\tilde{\mathbf{A}}^e$ for the solution domain Ω leads to the system of equations

$$\tilde{\mathbf{A}}\mathbf{u} = \mathbf{0} \tag{20}$$

in which the zero right-hand side indicates the absence of diffusive fluxes through the domain boundaries. In the above matrix equation vector $\mathbf{u}$ contains the unknown concentrations throughout Ω as well as the values prescribed at the Dirichlet space-time boundary conditions.

The problem may then be fully solved by a unique solution of system (20), but solving practical transient problems as steady-state generalized problems turns out to be difficult for general cases. However, given the space-time settings and a velocity field that is assumed to be constant over each time step, the final solution can be safely marched in time because space-time world-lines always have a positive component in the direction of time (i.e., $\beta > 0$). In doing so matrix $\tilde{\mathbf{A}}$ of

system (20) is established for a single space-time layer of width $\Delta\zeta$ to give

$$\tilde{\mathbf{A}}\mathbf{u} = \begin{bmatrix} \mathbf{P} & \mathbf{Q} \\ \mathbf{R} & \mathbf{S} \end{bmatrix} \begin{pmatrix} \mathbf{u}^t \\ \mathbf{u}^{t+\Delta t} \end{pmatrix} = \mathbf{0}, \tag{21}$$

where the vector $\mathbf{u}$ includes now only the known nodal value at time t and the unknowns at time $t + \Delta t$ when linear or multilinear elements are used in 2, 3, or 4D. Hence the solution for the time step is obtained by solving the reduced system

$$\mathbf{S}\mathbf{u}^{t+\Delta t} = -\mathbf{R}\mathbf{u}^t \tag{22}$$

and is used to update the flow field or is just fed back into the system until the final time is reached. We note here that matrix $\mathbf{S}$ above is symmetric, positive definite, and therefore the corresponding linear system can be solved with particularly efficient elliptic solvers.

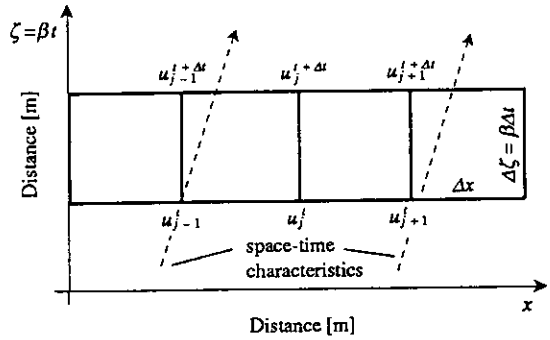

FIG. 2. Bilinear space-time layer for stability analysis.

Computational Behavior

In order to assess the computational properties of the proposed method and compare them to other schemes, we consider below a 2D (x, ζ) space-time layer discretized in bilinear square elements ($\Delta x = \Delta\zeta$) as depicted in Fig. 2. After integration, each element yields the 4×4 matrix

$$\tilde{\mathbf{A}}^e = \begin{bmatrix} \frac{v_x^2}{3} + \frac{\beta v_x}{2} + \frac{\beta^2}{3} & -\frac{v_x^2}{3} + \frac{\beta^2}{6} & -\frac{v_x^2}{6} - \frac{\beta v_x}{2} - \frac{\beta^2}{6} & \frac{v_x^2}{6} - \frac{\beta^2}{3} \\ * & \frac{v_x^2}{3} - \frac{\beta v_x}{2} + \frac{\beta^2}{3} & \frac{v_x^2}{6} - \frac{\beta^2}{3} & -\frac{v_x^2}{6} + \frac{\beta v_x}{2} - \frac{\beta^2}{6} \\ * & * & \frac{v_x^2}{3} + \frac{\beta v_x}{2} + \frac{\beta^2}{3} & -\frac{v_x^2}{3} + \frac{\beta^2}{6} \\ \text{sym} & * & * & \frac{v_x^2}{3} - \frac{\beta v_x}{2} + \frac{\beta^2}{3} \end{bmatrix}. \tag{23}$$

Dividing by β^2 and introducing the Courant number $Cr = v_x/\beta$ one obtains the adimensional form

$$\tilde{\mathbf{A}}^e = \begin{bmatrix} \frac{Cr^2}{3} + \frac{Cr}{2} + \frac{1}{3} & -\frac{Cr^2}{3} + \frac{1}{6} & -\frac{Cr^2}{6} - \frac{Cr}{2} - \frac{1}{6} & \frac{Cr^2}{6} - \frac{1}{3} \\ * & \frac{Cr^2}{3} - \frac{Cr}{2} + \frac{1}{3} & \frac{Cr^2}{6} - \frac{1}{3} & -\frac{Cr^2}{6} + \frac{Cr}{2} - \frac{1}{6} \\ * & * & \frac{Cr^2}{3} + \frac{Cr}{2} + \frac{1}{3} & -\frac{Cr^2}{3} + \frac{1}{6} \\ \text{sym} & * & * & \frac{Cr^2}{3} - \frac{Cr}{2} + \frac{1}{3} \end{bmatrix} \tag{24}$$

and after assembly of p elements the tridiagonal $(p + 1) \times (p + 1)$ matrices of system (22) produce the typical j^{th} equation

$$(1 - 2Cr^2)u_{j-1}^{t+\Delta t} + 4(1 + Cr^2)u_j^{t+\Delta t} + (1 - 2Cr^2)u_{j+1}^{t+\Delta t} = (1 + 3Cr + Cr^2)u_{j-1}^t + 2(2 - Cr^2)u_j^t + (1 - 3Cr + Cr^2)u_{j+1}^t. \tag{25}$$

Interestingly enough, for this simplified case, the above typical equation is the same as the one derived in [1] following a fairly different approach, although based on the least-squares method,

TABLE I

Phase Errors Δ in Units of Wavelength and Damping Factor G after One Oscillation of Each Mode

Cr	θ	Δ	G
0.2	$\pi/4$	0.0061	0.9717
	$\pi/2$	0.0544	0.7462
	$3\pi/4$	0.2923	0.2707
0.5	$\pi/4$	0.0251	0.9237
	$\pi/2$	0.0977	0.5220
	$3\pi/4$	0.2479	0.0910
0.9	$\pi/4$	0.0690	0.8447
	$\pi/2$	0.1825	0.4030
	$3\pi/4$	0.2371	0.1074
1.2	$\pi/4$	0.1096	0.7803
	$\pi/2$	0.2485	0.3775
	$3\pi/4$	0.2926	0.1703
1.6	$\pi/4$	0.1663	0.7009
	$\pi/2$	0.3288	0.3795
	$e\pi/4$	0.3880	0.2708
2.0	$\pi/4$	0.2211	0.6371
	$\pi/2$	0.3976	0.4000
	$3\pi/4$	0.4721	0.3618

in which neither a standard Galerkin integration is performed nor a steady-state anisotropic diffusion concept appears. Substituting in this recurrent relation a Fourier mode e^{ikx} (with wave number k and wavelength $\lambda = 2\pi/k$) so that $u_j^l = a(t)e^{ikj\Delta x}$, one obtains the eigenvalue $\gamma = a(t + \Delta t)/a(t)$, namely,

$$\gamma = \frac{2 - Cr^2 + (1 + Cr^2)\cos\theta - \hat{\imath}3Cr\sin\theta}{2 + 2Cr^2 + (1 - 2Cr^2)\cos\theta} \tag{26}$$

where $\theta = k\,\Delta x = 2\pi/n$ ($n = \lambda/\Delta x$) is the phase angle. It is easily seen that the scheme in Eq. (25) is unconditionally stable (i.e., $|\gamma| \leq 1\ \forall\ \theta, Cr$). After a complete oscillation the amplification factor and the phase error of the Fourier mode can be calculated by

$$G = |\gamma|^{2\pi/\theta Cr}, \quad \Delta = 1 - \frac{\cos^{-1}(\mathrm{Re}(\gamma/|\gamma|))}{\theta Cr} \tag{27}$$

for different θ and Cr values. Table I indicates that the proposed STILS-Galerkin method compares reasonably well with more sophisticated Petrov- and Taylor-Galerkin schemes (see, for example, [7, 9])—at least within their operational range $Cr < 1$ and specially for the domain of realistic space discretization $\theta \leq \pi/4$ (requiring a wavelength to be discretized by $n \geq 8$ elements).

The above classical Fourier analysis provides valuable insights to solution accuracy and stability. Nevertheless, our opinion is that this type of theoretical analysis does not take into account *all* of the numerical mechanisms involved in the practical solution process.

To better visualize the gain in computational robustness of the STILS-Galerkin approach, a complementary—and perhaps more realistic—stability analysis may indeed be performed on the full amplification matrix $\mathbf{G}$ that actually time marches the solution. The spectral norm of this matrix gives an indication on how fast over- or undershooting solution perturbations can be potentially amplified during time stepping. From system (22) we derive, assuming a constant coefficient problem,

$$\mathbf{G} = -\mathbf{S}^{-1}\mathbf{R}. \tag{28}$$

Unlike the theoretical amplification factor in Eq. (26) which depends on two variables, we can compute $\|\mathbf{G}\|$ as a function of Cr only. Figure 3 displays a comparison of the function $\|\mathbf{G}(Cr)\|$ for the standard Crank–Nicolson–Galerkin (CNG), streamline-upwind-Petrov–Galerkin (SUPG) [4], and Crank–Nicolson–Taylor–Galerkin (CNTG) [7] schemes. In these calculations we used $p = 20$ bilinear elements, $\|\mathbf{G}\|$ being not significantly influenced by p for $p > 10$. The amplification matrix for the CNG, SUPG, and CNTG schemes can be found in [15], together with some comments on the fact that $\|\mathbf{G}\|$ is never smaller than one for advective schemes.

Discussion

It follows from Fig. 3 that the proposed parabolic space-time formulation of advection leads to a scheme that suffers relatively low computational amplification of errors over a practical range of Cr numbers. Regarding the dramatic behavior of the CNTG amplification function, it might not be useless to

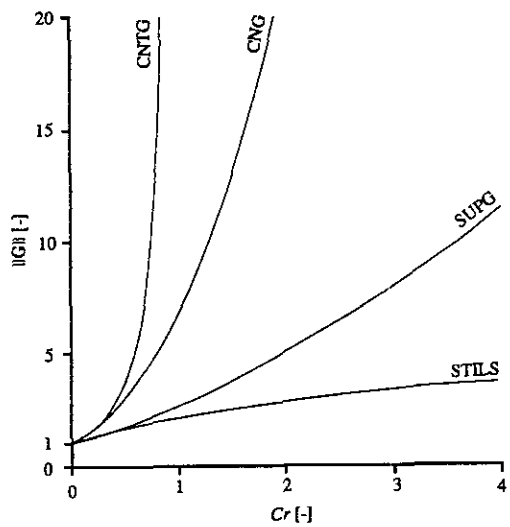

FIG. 3. Comparison of the norm of the amplification matrix $\mathbf{G}(Cr)$ for various advection schemes.

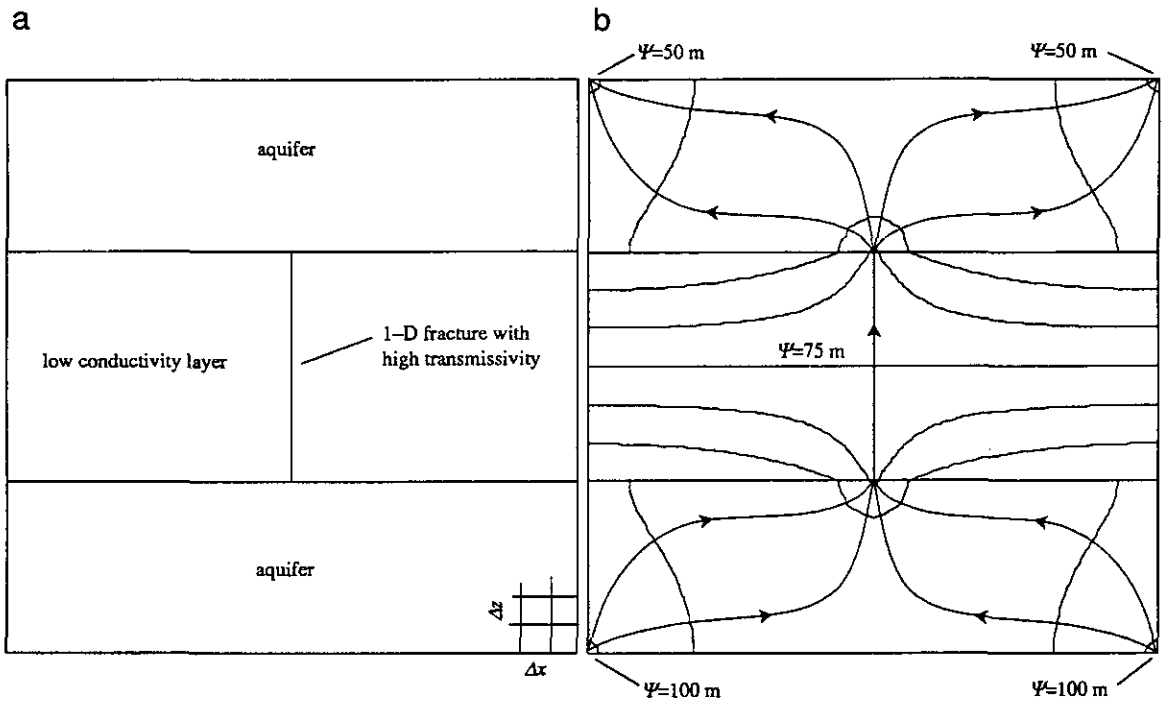

FIG. 4. Heterogeneous and fractured system: (a) domain structure and discretization; (b) input Laplacian flow field (equipotentials Ψ and streamlines) for advection simulation.

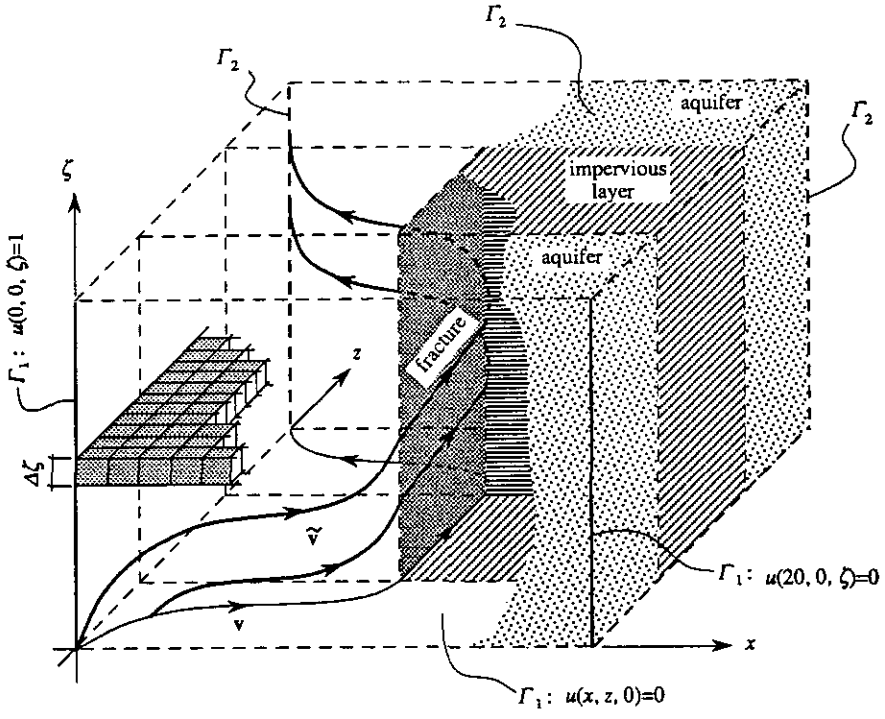

FIG. 5. 3D space-time representation of heterogeneities with characteristics (labeled $\tilde{\mathbf{v}}$), finite element "slab" of width $\Delta\zeta = \beta\,\Delta t$ and domain boundaries.

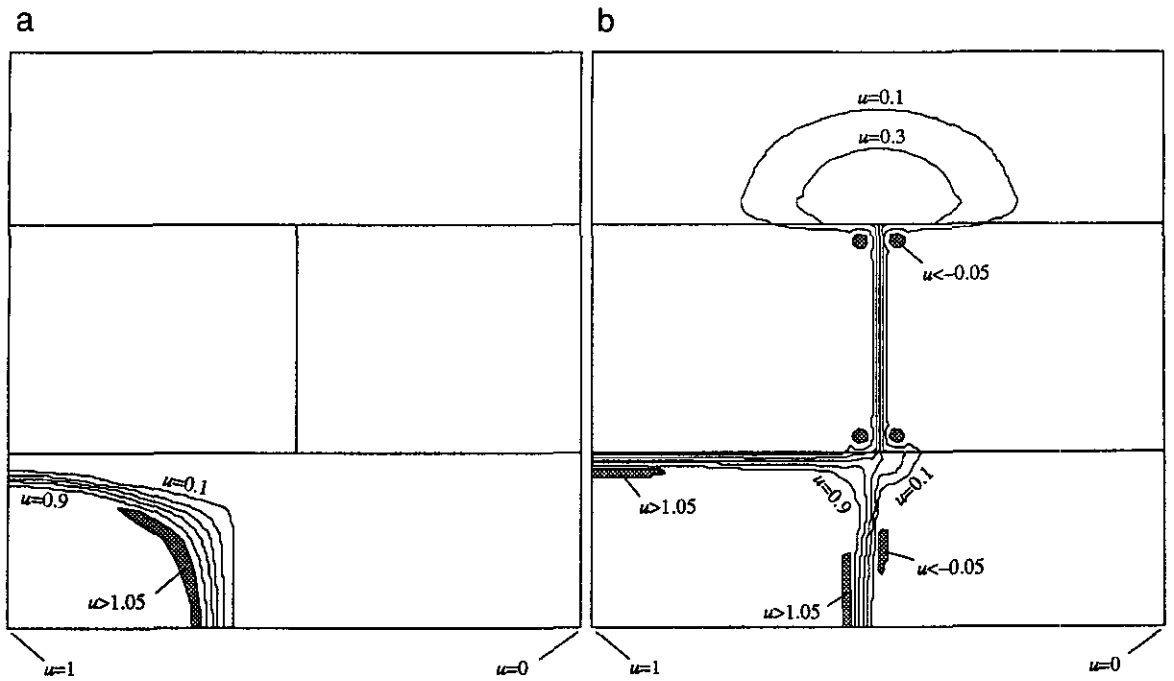

FIG. 6. Fractured "plug-flow" solutions: (a) after five time steps ($t^* = 10{,}000$ s); (b) after 10 time steps ($t^* = 20{,}000$ s).

mention that the CNTG unconditional stability arrived at in [7] using the Fourier mode analysis remains purely theoretical. As a matter of fact, the 1D CNTG matrix system becoming increasingly ill-conditioned for increasing Cr values in the range $0.5 < Cr < 1$ (with a singularity at $Cr = 1$) yields the asymptotic evolution of the curve $\|\mathbf{G}(Cr)\|$. Such a behavior clearly warns for the now well-experienced blowing up of instabilities, despite the higher orders of accuracy achieved by Taylor-Galerkin methods.

Obviously, the Fourier mode analysis ignores the "real," computational behavior of the CNTG scheme, which must unfortunately be used only in problems where a strict control over Cr is possible and affordable. Alternatively, the contemporary highly accurate Petrov–Galerkin schemes might as well be affected by this phenomenon. The latter seriously jeopardizes the implementation of these sophisticated methods for practical multidimensional problems (i.e., irregular and coarse meshes, heterogeneous flow fields, etc.) for which unknown stability conditions are expected to be most severe.

From a practical point of view and granted these considerations, we have to disagree here with the poor rating of the least-squares space-time method for pure advection problems given in the review article [8]; the statement was exclusively based on the results of the Fourier mode analysis. Consequently, in full accordance with our experiments and despite some theoretical weaknesses appearing only in the Fourier analysis, we can strongly recommend the present STILS-Galerkin approach for robust solutions of practical advective problems (see examples below). As a matter of fact, robustness seems to be provided by the consistent Galerkin treatment—or "proper balancing" [8]—of space and time derivatives in the symmetric, multidimensional proposed equation. In this context it is clear that introducing an artificial difference between steady-state and transient problems is not meaningful (see Eqs. (1) and (3)), since every component of the space-time characteristics and gradients can be represented properly and with equal accuracy in each of the four dimensions.

5. EXAMPLES

"Plug-Flow" in a Heterogeneous, Fractured Flow Field

We consider first a vertical domain composed of two layers of high conductivity material ($K = 10^{-3}$ m/s) hydraulically connected by a fracture through an intervening layer of very low conductivity ($K = 10^{-8}$ m/s) as shown in Fig. 4a. This (x, z) flow domain is discretized in 20×20 2D biquadratic elements ($\Delta x = \Delta z = 1$ m) and the fracture is identified by means of 1D highly transmissive quadratic elements ($Ke = 10^{-2}$ m^2/s, where e is the aperture of the fracture). Figure 4b illustrates the steady-state heterogeneous Laplacian flow field $\mathbf{v}$ generated under no-flow conditions on the sides of the domain and imposed hydraulic heads at the lower ($\Psi = 100$ m) and upper ($\Psi = 50$ m) corners.

Introducing the dimension ζ and specifying constant concentrations at the lower left ($u = 1$) and right ($u = 0$) corners, transient advection is then simulated with the suggested "steady-state" anisotropic diffusion operator. Figure 5 depicts

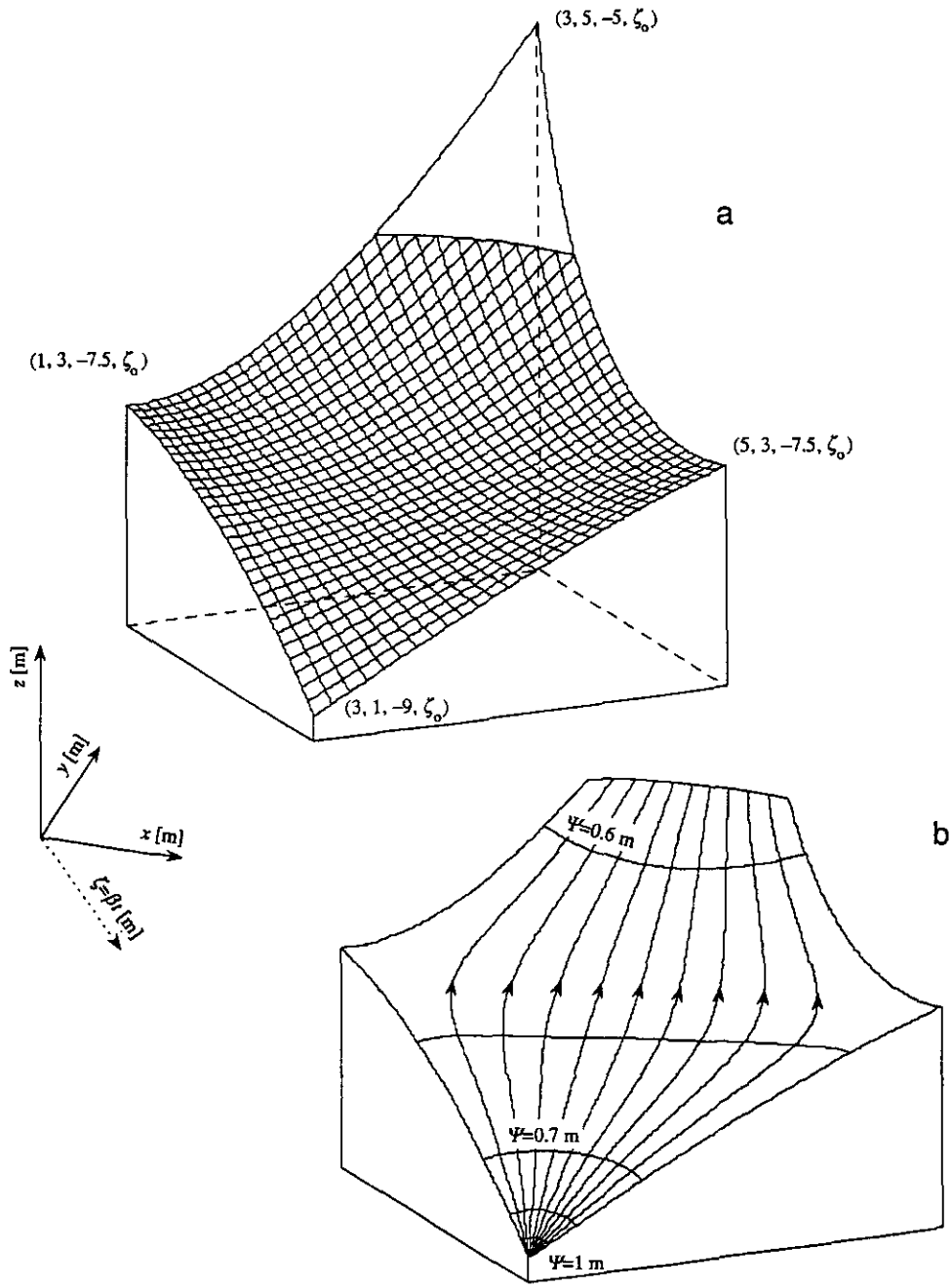

FIG. 7. 2D curved flow domain in 4D (x, y, z, z) space: (a) finite element mesh at an arbitrary time level $\zeta = \zeta_0$; (b) input Laplacian flow field (equipotentials Ψ and streamlines).

the 3D (x, z, ζ) domain and space-time streamlines, as well as the space-time upstream and downstream boundaries with Dirichlet (Γ_1) and zero Neumann conditions (Γ_2). From this figure it is understood that the heterogeneous structure of the space-time elementary layer (of thickness $\Delta\zeta$) is obtained by automatic generation of 2D and 3D elements from the 1D and 2D elements used for the (x, z) space discretization. The STILS-Galerkin solutions at $t^* = 10{,}000$ s and 20,000 s, obtained after only 5 and 10 time steps ($\Delta\zeta = 2$ m, $\Delta t = 2000$ s, $\beta = 10^{-3}$ m/s, are reported on Fig. 6. Each of these 2D concentration distributions (isolines) has to be interpreted as the intersection of the 3D space-time "block solution" (isosurfaces) with the plane (x, z, $\zeta = \beta t^*$).

Attempts to solve this problem with the higher order CNTG scheme—although using time steps that were reduced down to 500 times—only resulted in overflow messages obviously

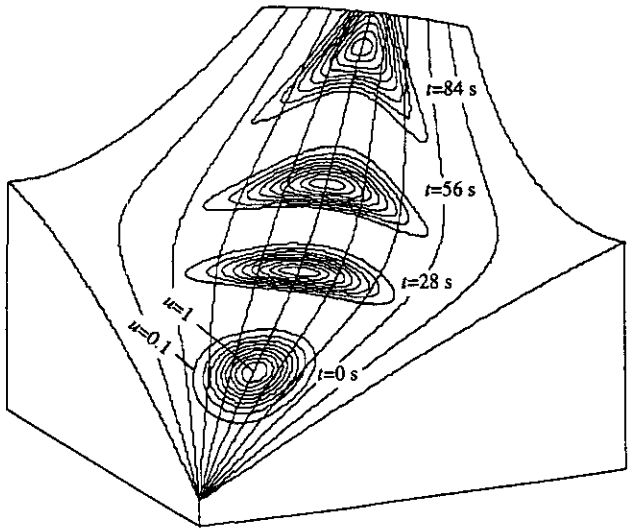

FIG. 8. Advection over a curved surface. Solutions at $t^* = 28$ s, 56 s, and 84 s with initial condition $u(x, y, z, 0) = \exp(-\{(x - 3.0512)^2 + (y - 1.8)^2\}/0.06)$.

due to local violations of some multidimensional drastic stability conditions in the regions of high velocities.

On the other hand, both of the concentration distributions on Fig. 6 show maximum "stable" irregularities of ± 7–8% due to the problematic interpolation of sharp fronts. However, the latter remain quite acceptable given the difficulty of the problem (coarse space-time discretization) and these realistic results can be reasonably interpreted. Since equal quantities of fluid are flowing in from the lower left and right corners, we note that after about 20,000 s of flow (Fig. 6b) full mechanical mixing is achieved by the fracture. Hence, past this time, the endpoint of the fracture acts as a constant point source with $u = 0.5$ in the upper layer where the front is much smoother due to the mixing effects.

Advection in a Diverging–Converging Flow Field over a Curved Surface

This second example consists of a surface with nonzero curvature embedded in the 3D space (x, y, z). The manifold is discretized as illustrated on Fig. 7a and a unity homogeneous conductivity is enforced ($K = 1$ m/s). The streamlines of the advective Laplacian flow field $\mathbf{v}$ given as input are shown on Fig. 7b. Since the three conventional dimensions are already used to represent this curved flow domain, we must work here in a 4D context to take time into account. To do so, 3D rectangular and triangular prisms are automatically generated in the ζ-direction on the base of the 2D curved quadrilaterals and triangular elements given on Fig. 7a.

Four-dimensional steady-state "parabolic advection" is then simulated in the resulting 3D curved domain with an upstream boundary $\zeta = 0$ m (i.e., $t = 0$ s) on which an "initial" Gaussian peak is specified. Space-time gradients and trajectories have, hence, four components, but the block-solution still consists of isosurfaces that may be intersected with "curved sections" $(x, y, z, \zeta = \beta t^*)$, that is, the solutions in the 2D manifold at given times t^*. The STILS-Galerkin results for this problem are shown on Fig. 8 at $t^* = 28$, 56, and 84 s. Using a time step of 2s ($\Delta\zeta = 2$ m, $\beta = 1$ m/s) numerical irregularities were smaller than ±1% at all times. We note on Fig. 8 the deformation of the initial Gaussian peak due to differential acceleration–deceleration effects and to the diverging–converging flow patterns. With the space-time discretization enforced in this example, it is seen that the intensity of the peak is preserved throughout the flow domain and that the deformed pulse leaves the mesh properly.

Seeking comparative results we tried to solve this "smooth front" problem with the CNTG scheme. Unfortunately, and even for quasi-infinitesimal time steps, the latter kept on delivering erratic solutions—if not overflow messages—due to spurious instabilities perhaps amplified by the curvature of the flow domain.

6. CONCLUSIONS

An original space-time diffusive-type model equation to solve purely advective multidimensional linear transport problems has been developed and analyzed in this work. Theoretical considerations regarding the equivalence of the advective equation with its diffusive counterpart are given and a new conceptual representation of transient advection is suggested. On the basis of a very classical steady-state finite element technique, the computational performances of the method are assessed in terms of stability, accuracy, and robustness.

The efficiency of this new space-time integrated least-squares approach and its related standard elliptic Galerkin algorithms is demonstrated by means of two rather difficult problems involving complex features, which could not be solved with the higher order numerical techniques at hand. Extension of the method to general nonlinear problems is now in progress and will be reported in due time.

ACKNOWLEDGMENTS

Funding for this work was provided by the Swiss National Science Foundation (FNRS). Special thanks are due to Professors Laszlò Kiraly, Olivier Besson, and François Zwahlen—all at the University of Neuchâtel—for stimulating discussions and substantial encouragements.

REFERENCES

1. H. Nguyen and J. Reynen, *Comput. Methods Appl. Mech. Eng.* **42,** 331 (1984).
2. G. F. Carey and B. N. Jiang, *Int. J. Numer. Methods Eng.* **26,** 81 (1988).
3. K. W. Morton and A. K. Parrott, *J. Comput. Phys.* **36,** 249 (1980).
4. A. N. Brooks and T. J. R. Hughes, *Comput. Methods Appl. Mech. Eng.* **32,** 199 (1982).

5. T. J. R. Hughes, L. P. Franca and G. M. Hulbert, *Comput. Methods Appl. Mech. Eng.* **73,** 173 (1989).
6. L. P. Franca and T. J. R. Hughes, *Comput. Methods Appl. Mech. Eng.* ***105,*** *285 (1993).*
7. J. Donea, *Int. J. Numer. Methods Eng.* **20,** 101 (1984).
8. J. Donea and L. Quartapelle, *Comput. Methods Appl. Mech. Eng.* **95,** 169 (1992).
9. L. Quartapelle, *Numerical solution of the incompressible Navier–Stokes equations,* Birkhäuser, Basel, 1993.
10. M. E. Cantekin and J. J. Westerink, *Int. J. Numer. Methods Eng.* **30,** 397 (1990).
11. C. Johnson, *Comput. Methods Appl. Mech. Eng.* **100,** 45 (1992).
12. P. Hansbo, *Comput. Methods Appl. Mech. Eng.* **96,** 239 (1992).
13. P. Hansbo, *Comput. Methods Appl. Mech. Eng.* **99,** 171 (1992).
14. P. Perrochet, *Int. J. Numer. Methods Eng.* **36,** 4165 (1993).
15. P. Perrochet, Ph.D. thesis No. 1046, Swiss Institute of Technology, Lausanne, Switzerland, 1992.
16. R. Temam, *Ann. Mat. Pura Appl.* **79,** 191 (1968).
17. R. Glowinski, *Numerical methods for nonlinear variational problems,* Springer-Verlag, New York/Berlin, 1984.